Two-dimensional talc as a van der Waals material for solid lubrication at the nanoscale

OPEN ACCESS
IOP Publishing
Nanotechnology

Nanotechnology **32** (2021) 265701 (10pp)
https://doi.org/10.1088/1361-6528/abeffe

Two-dimensional talc as a van der Waals material for solid lubrication at the nanoscale

Borislav Vasić[1,*], Caterina Czibula[2,3], Markus Kratzer[2], Bernardo R A Neves[4], Aleksandar Matković[2,*] and Christian Teichert[2]

[1] Institute of Physics Belgrade, University of Belgrade, Pregrevica 118, 11080 Belgrade, Serbia
[2] Institute of Physics, Montanuniversität Leoben, Franz Josef Strasse 18, A-8700 Leoben, Austria
[3] Institute of Bioproducts and Paper Technology, Graz University of Technology, Inffeldgasse 23, A-8010 Graz, Austria
[4] Departamento de Física, ICEx, Universidade Federal de Minas Gerais, 30123-970 Belo Horizonte, MG, Brazil

E-mail: bvasic@ipb.ac.rs and aleksandar.matkovic@unileoben.ac.at

Received 2 November 2020, revised 14 January 2021
Accepted for publication 18 March 2021
Published 6 April 2021

Abstract

Talc is a van der Waals and naturally abundant mineral with the chemical formula $Mg_3Si_4O_{10}(OH)_2$. Two-dimensional (2D) talc could be an alternative to hBN as van der Waals dielectric in 2D heterostructures. Furthermore, due to its good mechanical and frictional properties, 2D talc could be integrated into various hybrid microelectromechanical systems, or used as a functional filler in polymers. However, properties of talcas one of the main representatives of the phyllosilicate (sheet silicates) group are almost completely unexplored when ultrathin crystalline films and monolayers are considered. We investigate 2D talc flakes down to single layer thickness and reveal their efficiency for solid lubrication at the nanoscale. We demonstrate by atomic force microscopy based methods and contact angle measurements that several nanometer thick talc flakes have all properties necessary for efficient lubrication: a low adhesion, hydrophobic nature, and a low friction coefficient of 0.10 ± 0.02. Compared to the silicon-dioxide substrate, 2D talc flakes reduce friction by more than a factor of five, adhesion by around 20%, and energy dissipation by around 7%. Considering our findings, together with the natural abundance of talc, we put forward that 2D talc can be a cost-effective solid lubricant in micro- and nano-mechanical devices.

Supplementary material for this article is available online

Keywords: van der Waals materials, layered minerals, 2D talc, phyllosilicates (sheet silicates), nanofriction, atomic force microscopy

(Some figures may appear in colour only in the online journal)

1. Introduction

Tribological issues such as stiction, friction, and wear are responsible for a poor reliability of micro- and nano-mechanical devices [1]. Due to their continuous miniaturization, they need integral components with reduced dimensions. Therefore, very thin solid lubricants are required in order to reduce friction and wear of moveable mechanical

* Authors to whom any correspondence should be addressed.

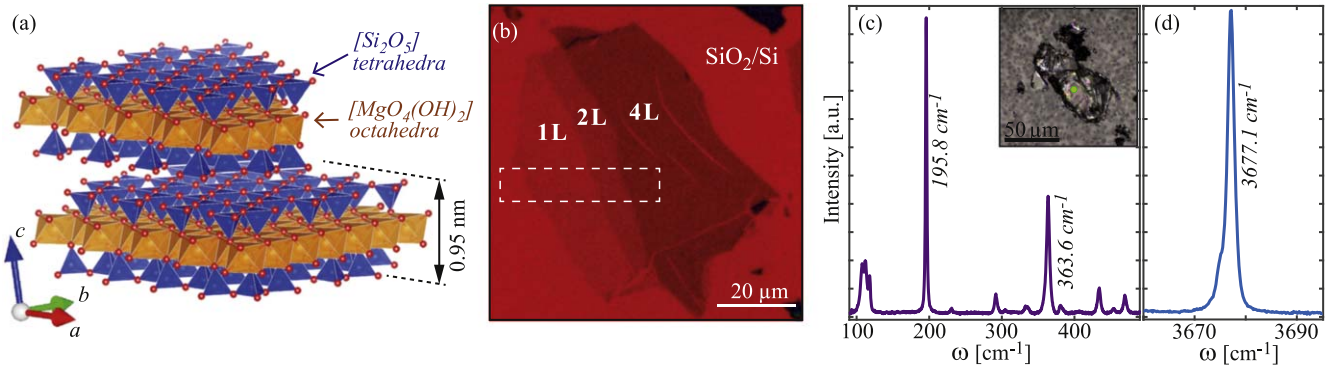

Figure 1. (a) Polyhedral structural model of talc, indicating a monolayer thickness of 0.95 nm. (b) Optical micrograph of a talc flake containing single-, bi-, and four-layer regions. Optical contrast is enhanced in order to highlight the mono-layer part of the flakes (see also figure S2 of supplementary material). Dashed white rectangle highlights the area where AFM topography measurements (presented in figure S2 of supplementary material) were used to confirm the flake thickness. (c) and (d) Raman spectra of a bulk talc flake: (c) modes that correspond to vibrations of Mg, (d) the Raman active mode of the -OH group. The inset in (c) provides an optical micrograph of the flake and its support. All Raman modes belong to the talc crystal, while exact frequencies are provided only for the most prominent ones for clarity.

parts in such devices. For that purpose, two-dimensional (2D) materials such as graphene, molybdenum disulfide, and hexagonal boron nitride are excellent candidates. Their Lamellar structure with weak van der Waals (vdW) forces between the layers enables easy shearing which results in low friction [2–4], while their crystal structure leads to preferential sliding directions [5–7] and superlubric sliding through incommensurate states [8–11]. Frictional properties and lubrication by 2D materials were extensively investigated in the last years [12–17], while most studies were focused on graphene demonstrating reduced friction [18, 19], wear [19–21], adhesion [18] and energy dissipation [22–24].

Recently, minerals such as franckeite [25–28], talc [29, 30], cylindrite [31] and serpentine [32] have attracted attention for the preparation of ultra-thin crystalline films and mono-layers. They extend the set of available vdW materials bringing novel and improved properties. For example, franckeite provides natural vdW heterostructures [25, 26] with possible applications in optoelectronic devices [27], whereas 2D cylindrite is an environmentally stable magnetic material [31].

Talc is a layered and naturally abundant mineral with the chemical formula $Mg_3Si_4O_{10}(OH)_2$. It belongs to the group of phyllosilicates. Talc is traditionally widely used as a filler, i.e. as a functional additive for various polymers in order to improve their mechanical properties [33–36]. Similar to graphite, molybdenum disulfide, and boron nitride, it has been also used as a lubricant in its bulk form for decades [37] and as an oil additive for friction reduction [38]. Geophysical studies revealed that the presence of talc decreases frictional strength of minerals [39, 40] and reduces the friction during sliding of crustal faults (planar fractures of rocks) with a strong influence on their seismic potential [41, 42]. Recently, mechanical [29] and liquid-phase [43] exfoliation have been used to obtain 2D talc flakes down to single layer thickness which is 0.95 nm. It was demonstrated that 2D talc is atomically flat [44] with good mechanical properties, a high breaking strength and elasticity [29]. The single layer of talc consists of the central $[MgO_4(OH)_2]$ octahedra 'sandwiched' between $[Si_2O_5]$ tetrahedra, see figure 1(a). Such Lamellar structure facilitates easy shearing between the layers, the feature responsible for a good lubrication of the bulk form. However, frictional properties of 2D talc at the nanoscale have not been investigated so far.

In this paper, we study adhesion, friction, and energy dissipation of 2D talc crystals using atomic force microscopy (AFM) based methods. Force–displacement curves [45] have been recorded to obtain values for the adhesion. The frictional behavior has been characterized by friction force microscopy [46], whereas phase imaging in tapping AFM mode [47–49] has been applied to investigate energy dissipation. We demonstrate that 2D talc has a low friction coefficient of only 0.10 ± 0.02. Compared to the surrounding silicon-dioxide substrate, the 2D talc reduces friction by 5-6 times, whereas the adhesion and energy dissipation are decreased by around 20% and 7%, respectively. These results demonstrate that 2D talc can be a cost-effective solid lubricant at the nanoscale.

2. Experimental methods

2.1. Sample preparation

Monolayer and multilayer talc flakes were prepared by micromechanical exfoliation using Nitto Denko ELP BT150ECM sticky tape. The shematics of the preparation process is presented in figure S1 of supplementary material (available online at stacks.iop.org/NANO/32/265701/mmedia). As the starting material, two different sources of natural talc mineral were used: 'soap-stone' crystals from Styria in Austria and pure steatite single crystals from Minas Gerais state in Brazil. Bulk talc flakes were deposited onto Si wafers with 300 nm thick SiO_2 layer. Figure 1(b) shows an example of the prepared flakes. Labeled thicknesses were determined by AFM. Areas with potential mono- and multilayers (up to ≈30 layers) were selected by optical microscopy. Optical contrast of ultra-thin talc flakes on such

support is similar to those of hexagonal boron nitride on SiO_2 [50, 51].

2.2. Raman characterization

Raman spectroscopy was employed to confirm that the deposited material is talc with high crystallinity. A Horiba LabRam HR Evolution co-local Raman spectrometer was used with EMCCD detector, 532 nm laser (100 mW power on the sample surface), 100× magnification lens, and 1800 lines mm^{-1} grating. Since talc has low Raman response —especially if compared to graphene—rather high acquisition times were used, from 20 s in the case of bulk up to 1200s for the flakes thinner than 10 nm. No sample damage was observed after prolonged exposure to the laser beam, which was confirmed by repeated Raman measurements and by AFM. Raman spectra were corrected for the background signal (obtained from the measurements of the nearby substrate) and cosmic rays were removed.

Figures 1(c), (d) presents Raman spectra of a bulk talc flake (shown in the inset of (c)) in the ranges of 100–500 cm^{-1} and 3660–3695 cm^{-1}, respectively. Vibrational modes of Mg were observed at lower frequencies (up to 900 cm^{-1}) [52]. Sharp vibrational mode of –OH group was observed at 3677 cm^{-1} [52]. Characteristic modes of water (3400–3600 cm^{-1} range) intercalating phyllosilicate structure were not observed. Bulk crystals were fixed on the tape which was used for the subsequent exfoliation of the same crystals. In such case, very low background signal was observed and modes of the supporting tape did not overlap with any characteristic modes of talc. All the modes presented in figures 1(c), (d) belong to talc vibrations and are in accordance with the data in the literature [52].

In the case of thin flakes on SiO_2/Si support (as shown in figure 1(b)), due to higher background signal and Si and SiO_2 modes which partly overlap with the modes of talc, only the most prominent modes at 195.8 cm^{-1}, 363.6 cm^{-1}, and 3677 cm^{-1} were clearly observed. For the flakes thinner than ≈10 layers only the characteristic mode of the OH vibrations was clearly observed, mainly since very low background signal at high frequencies allows for a much higher acquisition time. Results from Raman spectroscopy together with AFM and optical microscopy indicate that investigated talc samples are high-quality single crystals.

2.3. Water contact angle measurements of talc single crystals

Contact angle (CA) measurements have been performed with a Kruess DSA100 (Hamburg, Germany) at ambient conditions (23 °C and 55% relative humidity). For the investigation, water as a polar liquid ($\sigma_P = 50$ mN m^{-1}, $\sigma_D = 21.8$ mN m^{-1}) has been chosen. Water droplets with a volume of 1 μl have been deposited on the surface of SiO_2 and talc. Immediately afterwards, the CA has been evaluated via circle fitting in the Kruess Drop Shape Analysis software. For each substrate, four measurements have been performed. The values are given as mean, including standard deviation.

To provide a more realistic comparison with respect to exfoliated ultra-thin flakes, both samples for CA measurements were prepared in the manner which mimics the exfoliated flakes. For the SiO_2/Si, the chips were treated identically as for the exfoliation process, with the exception that only a bare tape was used instead of the tape containing talc flakes. For the talc samples, large-area, flat single crystals were chosen, with sample size of ≈8 × 8 mm^2. The surface was cleaved approximately 15 min prior to CA experiments, and the water droplets were deposited on areas where no features were observed on the surface by optical microscopy. During measurements, we have been careful in selecting only optically smooth and single-crystal talc surfaces which are significantly larger than water droplets. In this way we avoided any significant influence of local surface roughness variations on the obtained contact angle.

2.4. AFM measurements

AFM characterization of talc flakes was done by NTEGRA Prima AFM system from NT-MDT at ambient conditions. Nanoscale friction was measured by friction (lateral) force microscopy. Lateral force signals were measured during the imaging in contact AFM mode. These signals correspond to the lateral torsion of the AFM cantilever due to the friction between the AFM tip and sample surface during scanning. The friction signal was calculated as a half-difference between the lateral force signals measured in the forward and backward scan-directions. Calibration of the AFM cantilevers and the transformation of the measured friction signals into friction forces was done according to the well-established procedure described in [53]. Two different kinds of probes were used for friction measurements, moderately soft CSG10 and moderately stiff NSG01 probes from NT-MDT, with typical force constants of around 0.11 N m^{-1} and 5.1 N m^{-1}, respectively, and nominal tip curvature radius <10 nm.

Adhesion was determined from AFM based force–displacement curves obtained by the measurement of the AFM cantilever's normal deflection as a function of the vertical extension of the AFM scanner. The adhesion was calculated as the pull-off force needed to separate the AFM tip from the sample surface during tip retraction. Soft CSG01 probes from NT-MDT, with a typical force constant of around 0.03 N m^{-1} were used for that purpose. For each talc flake thickness, a 5 × 5 matrix of force–displacement curves was recorded on the flake as well as on the surrounding SiO_2 substrate. A value for the adhesion force was calculated by averaging each data set consisting of 25 measurement points.

Dissipation of the mechanical energy was determined in repulsive tapping AFM mode by measuring the phase lag of the AFM cantilever with respect to the phase of the piezo-excitation during the imaging. The phase lag originates from the tip-sample interaction which is controlled by a predefined set-point. A lower (higher) set-point means stronger (weaker) tip-sample interaction and reduced (enlarged) the AFM tip oscillation amplitude. The corresponding energy dissipation was calculated from the phase signal Φ according to the

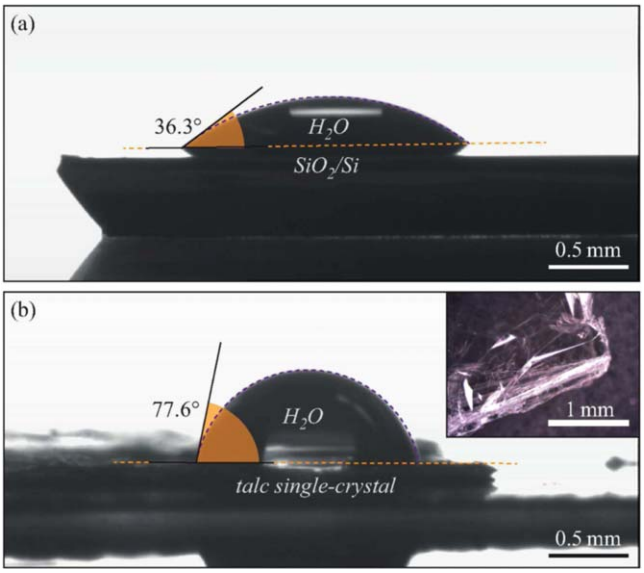

Figure 2. An example of the water CA measurements on (a) SiO_2/Si wafer and (b) talc single-crystal. Inset of (b) shows a low-magnification optical microscope image of one corner of the talc crystal which was used in the CA experiment presented in (b).

following formula [48, 49]

$$E_{\mathrm{dis}} = \frac{\pi k A A_0}{Q}\left(\sin\Phi - \frac{A}{A_0}\right), \tag{1}$$

where A and A_0 are amplitude and free-oscillation amplitude of AFM cantilever oscillations, respectively, k is force constant of the AFM cantilever, whereas Q is its quality factor which is around 200. The amplitude ratio A/A_0 is proportional to the amplitude set-point in tapping AFM mode, thus lower (larger) A/A_0 means stronger (weaker) tip-sample interaction.

3. Results and discussion

Good lubrication requires surfaces with a low adhesion. Despite of intriguing wetting properties of talc, at ambient conditions it is hydrophobic [54–57] with a water CA of around 80° [54, 58, 59]. Hydrophobicity of talc should facilitate easier sliding between two contacting surfaces and contribute to better lubrication. Wetting properties of talc were first tested by water CA measurements on both SiO_2/Si wafers and talc crystals. On the silicon oxide surface, a contact angle of $(39 \pm 7)°$ has been obtained (figure 2(a)). This result is similar to literature values [60]. Compared to that, on the talc surface, a contact angle of $(80 \pm 24)°$ has been measured, again in a good agreement with literature [54, 58, 59]. It should be noted that the surface of the talc sample under investigation has a higher roughness than that of the SiO_2/Si wafer (which can be also seen in figure 2(b)), therefore, the deviation in the results is higher. However, the results for the contact angles clearly reveal that the talc surface is less wettable with water, and therefore, more hydrophobic than the SiO_2 surface.

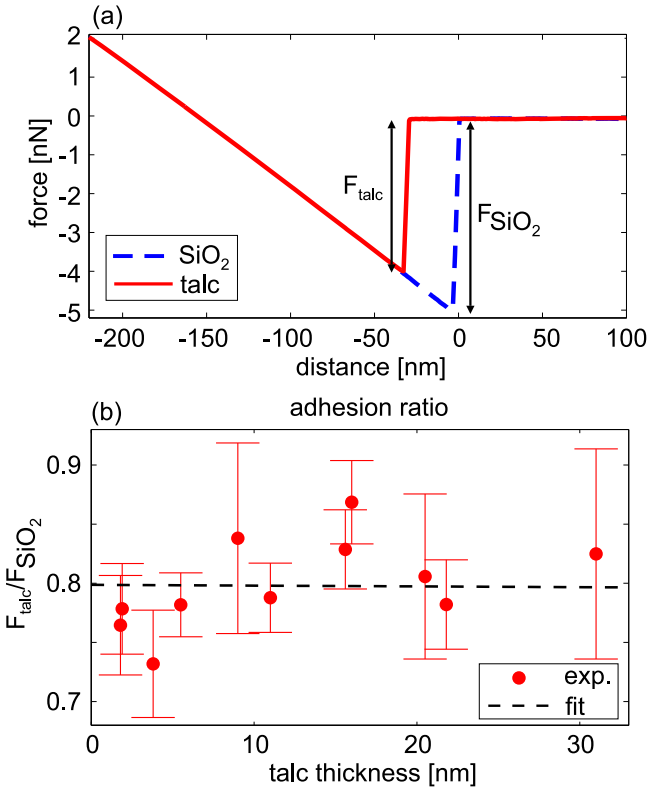

Figure 3. (a) Typical force–displacement curves measured by AFM. The adhesion force is calculated from the force–displacement curves as a pull-off force. (b) The ratio of adhesion forces measured on talc and the silicon-dioxide substrate as a function of the thickness of the talc flakes.

In order to test the adhesive properties of 2D talc flakes at the nanoscale, force–displacement curves were measured by AFM. Typical results are presented in figure 3(a). The adhesion force is marked as a pull-off force needed to separate the AFM tip from a surface and to overcome capillary forces due to an adsorbed water layer. As can be seen, the pull-off force is smaller on the talc covered SiO_2 substrate.

The ratio between adhesion force measured on 2D talc flakes and bare substrate is presented in figure 3(b) as a function of the thickness of talc flakes in the range of around 2–30 nm. Each point on the graph was obtained by averaging adhesion forces calculated from 25 force–displacement curves measured on the same flake. The average adhesion ratio of around 0.80 ± 0.12 means that the talc flakes reduce adhesion by around 20%. Such efficiency in adhesion reduction is similar to the one achieved by CVD graphene [18]. Adhesion measurements demonstrate that 2D talc is more hydrophobic than the surrounding silicon-dioxide substrate. This is in full accordance to the results obtained by CA measurements which reveal that talc is more hydrophobic than the SiO_2 surface. Therefore, the capillary adhesion is less pronounced which should facilitate lubrication. The experimentally measured points were fitted by a linear function represented by the dashed line. As can be seen, the fit is practically a horizontal line (slope of 10^{-4}) indicating that the adhesion force does not depend on the thickness of the talc flakes.

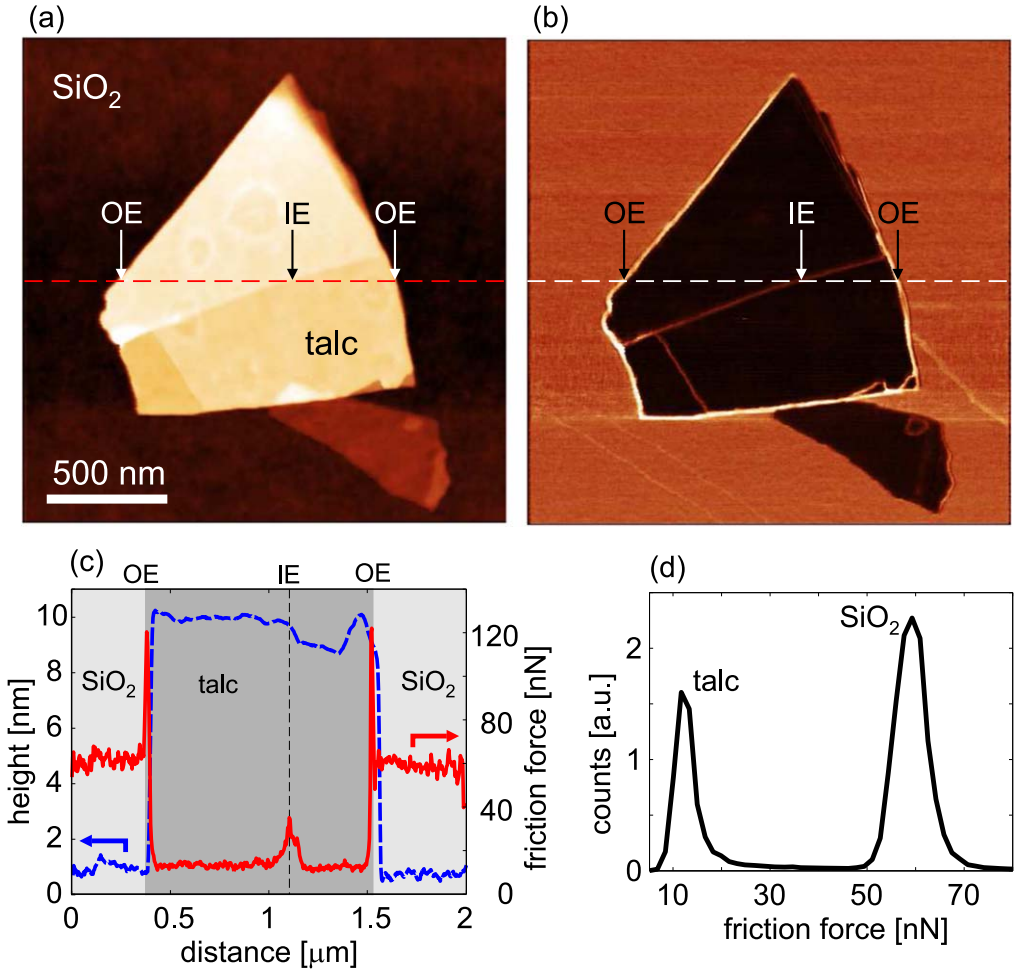

Figure 4. (a) Topography and (b) friction map of the talc flake which is characterized with four height levels (z-scales are 0–11 nm and 7.5–136.5 nN, respectively). Scanning was performed at a normal load $F_N = 138.4$ nN. (c) Cross-section of the topography and friction map along the dashed lines in (a) and (b). OE and IE stand for outer and inner talc edges, respectively. (d) Histogram of the friction map with two peaks corresponding to the friction of talc and bare silicon-dioxide substrate.

Topography and friction map of a typical multilayer talc flake recorded at a constant normal force $F_N = 138.4$ nN are presented in figures 4(a) and (b), respectively. Dark contrast of the talc flake in the friction map indicates decreased friction. Cross-section and histogram of the friction map, depicted in figures 4(c) and (d), respectively, provide more quantitative information. The friction force on the talc flake is around five times lower than on the bare SiO_2 substrate demonstrating very good lubricating properties. Although the talc flake consists of domains with different thickness, the friction on talc is rather homogeneous, characterized by an almost flat line in the friction force cross section and a narrow peak in the histogram, which indicates a weak dependence of the friction on the thickness of 2D talc.

Figure 4(c), with topography and friction profiles, displays that the friction peaks correspond to outer (transitions talc/substrate at a distance of around 0.4 and 1.5 μm) and inner talc edges (the inner step-height transition at a distance of around 1.1 μm between two parts with different thickness of around 1 nm). They are denoted with OE (outer edge) and IE (inner edge), respectively. It is well known that atomic step edges in both bulk [61, 62] and 2D layered materials [63–67] are associated with enhanced friction which leads to decreased wear resistivity [68, 69]. In the case of non-exposed graphene edges (buried edges covered by graphene layer(s) on top), the friction originates from topographic effects, whereas in the case of exposed edges (bare and uncovered edges exposed to environment), the friction is much more pronounced due to chemically reactive dangling bonds [63, 65–67]. Similar reasoning should be applicable in order to explain the increased friction along talc edges, but a detailed study of the effect is beyond the scope of this manuscript.

The friction maps were measured on the same talc flake as a function of the normal load. For each normal load, the average friction forces for both talc flake and the substrate were calculated from corresponding histograms. The final results are presented in figure 5. The friction forces increase approximately linearly with the normal load whereas their slopes correspond to the friction coefficients. Accordingly, the friction coefficient on talc is 0.11, and it is almost six times lower than on silicon-dioxide (around 0.59) which confirms excellent lubricating properties of 2D talc.

In order to test the dependence of friction on the thickness of talc flakes, the same measurements and analyses were

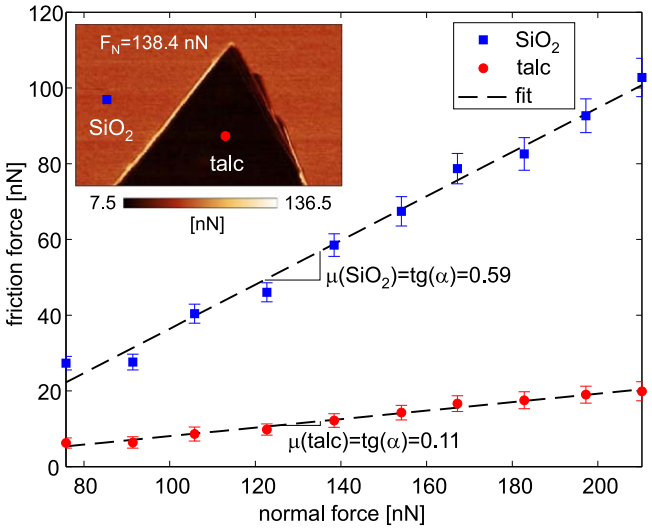

Figure 5. Friction force on talc and silicon-dioxide substrate as a function of the normal load applied by the AFM tip. Data were calculated for the talc flake (with a thickness of 9 nm) from the friction map (recorded at a normal load $F_N = 138.4$ nN) in the inset. Friction coefficients were determined from the slope of linear fits.

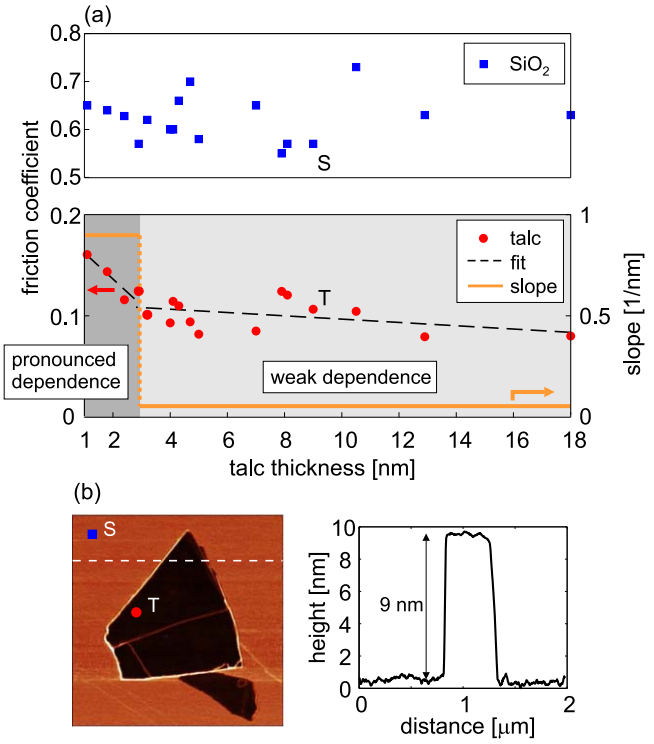

Figure 6. (a) Friction coefficient of talc flakes as a function of their thickness. Dashed line is linear fit, whereas the slope of the friction coefficient versus flake thickness (absolute value) is presented by the solid line. The experimental points are fitted by two linear parts with pronounced (darker region) and weak dependence (brighter) on the thickness. For each talc flake with a given thickness, the measured friction coefficient of surrounding SiO_2 is presented in the top panel. (b) As an illustration, the friction map (left) with the height profile (right) along the dashed line used to calculate points T and S from part (a), obtained for the talc thickness of 9 nm.

performed on different flakes (most of them with multiple height levels). As a result, the friction coefficient for the talc thickness in the range 1–18 nm is depicted in figure 6(a). For each talc flake with a given thickness, the friction coefficient of surrounding SiO_2 was measured as well with the results presented in the top panel of figure 6(a) in order to illustrate clear friction reduction by talc flakes (a bit larger data dispersion for SiO_2 originates probably from non-uniformly distributed contamination during exfoliation). Figure 6(b) illustrates the pair of points T and S corresponding to talc and SiO_2, respectively, for the talc thickness of 9 nm. The experimental points for the talc were fitted by two linear segments. The friction coefficient of talc significantly decreases from 0.16 to 0.1 for the thickness from 1 to 3 nm (1–3 talc layers). In this region with a pronounced dependence (darker region in figure 6(a)), the slope (absolute value) of the friction coefficient versus flake thickness is 0.9. On the other hand, for thicker flakes, from 3 to 18 nm, the friction coefficient is only weakly dependent on the thickness (brighter region in figure 6(a)), with the linear slope of 0.06 (absolute value), which is more than one order of magnitude lower than in the previous segment. The talc friction coefficient practically saturates for thicknesses >3 layers with a low value of only 0.10 ± 0.02. This value is similar to the case of chemical vapor deposited graphene on copper [18], while talc is a dielectric and therefore applicable in the cases where insulating layers are required. The value obtained for the friction coefficient of 2D talc is in accordance with the measurements of a bulk talc with the friction coefficient in a range 0.1–0.4 [70–72].

According to the presented results, friction of talc reduces with increasing material thickness in a similar way as other 2D materials [12], although slower compared to graphene and especially to molybdenum-disulfide and hexagonal boron-nitride. Generally, the friction of 2D materials decreases with increasing thickness because of the puckering effect [12] and local out-of-plane deformations [73], which are explained as follows. During the sliding of the AFM tip, 2D material becomes locally wrinkled below the tip which effectively increases the contact area and friction [12]. Thicker flakes have larger bending rigidity, and they are less prone to local puckering and out-of-plane deformations which results in a lower friction. A single talc layer is already around 1nm thick, which is almost three times thicker than graphene with the nominal thickness of 0.34 nm. A talc layer consists of three planes: one plane comprises $[MgO_4(OH)_2]$ octahedra, which are 'sandwiched' between two planes containing $[Si_2O_5]$ tetrahedra. Numerical calculations have demonstrated that the bending rigidity of a talc layer is more than thirty times larger than that of graphene [29]. Therefore, the puckering effect and deformation of talc flakes should be less pronounced which is likely the reason behind the observed weaker dependency of the friction coefficient on talc thickness compared to graphene, molybdenum-disulfide, and hexagonal boron-nitride.

During the sliding of the AFM tip in continuous contact with the underlying surface, the dominant dissipation mechanism of the mechanical energy is related to friction. Energy dissipation also takes place when the AFM tip oscillates

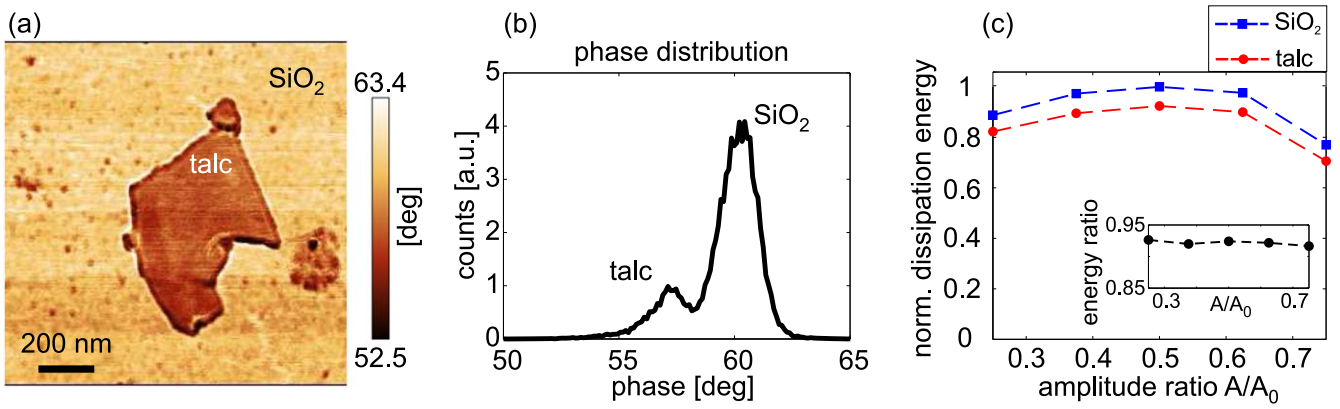

Figure 7. (a) Phase map of a talc flake (with a thickness 2.2 nm) acquired during tapping AFM mode imaging. (b) Histogram of the phase map. (c) Normalized dissipation energy as a function of the AFM amplitude ratio. The inset depicts the ratio between the energy dissipated on talc and bare silicon-dioxide substrate.

against the substrate as is the case in semi-contact (tapping) mode AFM. In order to measure the dissipation in such a case, the imaging in semi-contact (tapping) AFM mode was used. In tapping mode, the AFM tip is moving horizontally and simultaneously oscillating above the sample surface in the normal direction, while touching the surface once per each oscillation period. The dissipation energy is obtained from the simultaneously acquired phase signal according to equation (1).

A typical phase map of a 2D talc flake is displayed in figure 7(a), whereas the corresponding histogram is given in figure 7(b). As can be seen, the flake is darker, with a phase lag Φ lower by around 3° (calculated as a phase difference between two peaks in the histogram) than the phase measured on the bare silicon-dioxide substrate. Since the energy dissipation is proportional to $\sin(\Phi)$ (according to equation (1)), it exhibits a lower value on the talc flake. The same measurements and calculations were done for several amplitude ratios A/A_0. Corresponding results for the normalized energy dissipation calculated by equation (1) for both talc flake and bare SiO_2 substrate are shown in figure 7(c). The energy is represented as a function of the amplitude ratio A/A_0 which is inversely proportional to the strength of the AFM tip-substrate interaction. As can be seen, the dissipation is lower for a talc covered substrate. The ratio between the energy dissipated on the talc and the bare SiO_2 substrate, depicted in the inset of figure 7(c), is rather constant, around 0.92–0.93, meaning that the talc decreases dissipation by around 7%–8%. Similar levels of efficiency in reducing energy dissipation was demonstrated in the cases of graphene covered platinum and silicon-dioxide substrates as well [23, 24].

According to the concave, but also rather flat shape of the energy dissipation curve in figure 7(c), dominant dissipation mechanisms during tapping mode imaging are related to a combination of long-range vdW forces [48] and short-range surface hysteresis and capillary forces [48, 74]. It was demonstrated both experimentally [75] and theoretically [76, 77] that graphene and other 2D materials partially screen vdW interactions. Although this screening is less efficient for insulating graphene-like materials [77], it is reasonable to expect that talc as a 2D insulator is also partially opaque for vdW interactions, the property which is then responsible for lower dissipation due to long-range interactions in dynamic AFM modes. At the same time, reduced adhesion on talc-covered areas, as we have shown, contributes to lower surface energy hysteresis and capillary forces.

4. Conclusions

In summary, we have demonstrated that 2D talc flakes thicker than 3 nm (3 monolayers) have a low friction coefficient of only 0.10 ± 0.02, which weakly depends on the flake thickness. With reduced thickness (<3 nm), the friction coefficient increases reaching a maximum of 0.16 for a monolayer flake ~1 nm. Compared to silicon-dioxide substrate, talc flakes reduce friction by more than a factor of five, CA is increased by more than a factor of two, while adhesion and energy dissipation are reduced by around 20% and 7%, respectively. Therefore, 2D talc has all properties necessary for efficient lubrication. The obtained results indicate that the efficiency of talc flakes for nanoscale lubrication is very similar to chemical vapor deposited graphene, while being dielectrics, they are applicable in the cases where insulating layers are required. The natural abundance of talc mineral makes it a cost-effective source of 2D flakes which can be easily exfoliated due to the vdW nature of the mineral. Therefore, 2D talc is a promising and also cost-effective candidate for lubrication at the nanoscale.

Acknowledgments

B V acknowledges funding provided by the Institute of Physics Belgrade, through the grant of the Ministry of Education, Science, and Technological Development of the Republic of Serbia and support by the Science Fund of the Republic of Serbia, PROMIS 6062710, PV-Waals. We also acknowledge support by the Austrian Academic Exchange Service (OeAD) (via the project SRB 13/2018) and the

Ministry of Education, Science, and Technological Development of the Republic of Serbia (via the project 451-03-02141/2017-09/32) through the bilateral project between Republic of Austria and Republic of Serbia. A M acknowledges the support of the START Programme by the Austrian Science fund (FWF) (grant no. Y 1298). B R A N acknowledges financial support from FAPEMIG, CNPq and INCT-NanoCarbono. C C acknowledges financial support of the Christian Doppler Laboratory for Fiber Swelling and Paper Performance located at Graz University of Technology which is supported by the Austrian Federal Ministry for Digital and Economic Affairs and the National Foundation for Research Technology and Development. The authors acknowledge infrastructural support of the Raman-TERS lab at Montanuniversität Leoben. We thank Prof. Ronald J. Bakker (Montanuniversität Leoben) for providing 'soap stone' minerals.

Data availability statement

All data that support the findings of this study are included within the article (and any supplementary files).

ORCID iDs

Borislav Vasić https://orcid.org/0000-0002-1575-8004
Caterina Czibula https://orcid.org/0000-0002-7962-5796
Markus Kratzer https://orcid.org/0000-0001-5181-6796
Bernardo R A Neves https://orcid.org/0000-0003-0464-4754
Aleksandar Matković https://orcid.org/0000-0001-8072-6220
Christian Teichert https://orcid.org/0000-0002-0796-2355

References

[1] Achanta S and Celis J-P 2015 *Fundamentals of Friction and Wear on the Nanoscale, chapter Nanotribology of MEMS/NEMS* (Switzerland: Springer International Publishing)
[2] Berman D, Erdemir A and Sumant A V 2018 Approaches for achieving superlubricity in two-dimensional materials *ACS Nano* **12** 2122–37
[3] Zhang S, Ma T, Erdemir A and Li Q 2019 Tribology of two-dimensional materials: from mechanisms to modulating strategies *Mater. Today* **26** 67–86
[4] Liu L, Zhou M, Jin L, Li L, Mo Y, Su G, Li X, Zhu H and Tian Y 2019 Recent advances in friction and lubrication of graphene and other 2D materials: Mechanisms and applications *Friction* **7** 199–216
[5] Feng X, Kwon S, Park J Y and Salmeron M 2013 Superlubric sliding of graphene nanoflakes on graphene *ACS Nano* **7** 1718–24
[6] Sheehan P E and Lieber C M 2017 Friction between van der Waals solids during lattice directed sliding *Nano Lett.* **17** 4116–21
[7] Vasić B, Stanković I, Matković A, Kratzer M, Ganser C, Gajić R and Teichert C 2018 Molecules on rails: friction anisotropy and preferential sliding directions of organic nanocrystallites on two-dimensional materials *Nanoscale* **10** 18835–45
[8] Dienwiebel M, Verhoeven G S, Pradeep N, Frenken J W M, Heimberg J A and Zandbergen H W 2004 Superlubricity of graphite *Phys. Rev. Lett.* **92** 126101
[9] Liu Z, Yang J, Grey F, Liu J Z, Liu Y, Wang Y, Yang Y, Cheng Y and Zheng Q 2012 Observation of microscale superlubricity in graphite *Phys. Rev. Lett.* **108** 205503
[10] Kawai S *et al* 2016 Superlubricity of graphene nanoribbons on gold surfaces *Science* **351** 957
[11] Song Y, Mandelli D, Hod O, Urbakh M, Ma M and Zheng Q 2018 Robust microscale superlubricity in graphite/hexagonal boron nitride layered heterojunctions *Nat. Mater.* **17** 894–9
[12] Lee C, Li Q, Kalb W, Liu X-Z, Berger H, Carpick R W and Hone J 2010 Frictional characteristics of atomically thin sheets *Science* **328** 76–80
[13] Li X, Yin J, Zhou J and Guo W 2014 Large area hexagonal boron nitride monolayer as efficient atomically thick insulating coating against friction and oxidation *Nanotechnology* **25** 105701
[14] Ky D L C, Tran Khac B-C, Le C T, Kim Y S and Chung K H 2018 Friction characteristics of mechanically exfoliated and CVD-grown single-layer MoS_2 *Friction* **6** 395–406
[15] Lavini F, Calò A, Gao Y, Albisetti E, Li T-D, Cao T, Li G, Cao L, Aruta C and Riedo E 2018 Friction and work function oscillatory behavior for an even and odd number of layers in polycrystalline MoS_2 *Nanoscale* **10** 8304–12
[16] Vazirisereshk M R, Ye H, Ye Z, Otero-de-la Roza A, Zhao M-Q, Gao Z, Johnson A T C, Johnson E R, Carpick R W and Martini A 2019 Origin of nanoscale friction contrast between supported graphene, MoS_2, and a graphene/MoS_2 heterostructure *Nano Lett.* **19** 5496–505
[17] Tran-Khac B-C, Kim H-J, DelRio F W and Chung K-H 2019 Operational and environmental conditions regulate the frictional behavior of two-dimensional materials *Appl. Surf. Sci.* **483** 34–44
[18] Kim K-S *et al* 2011 Chemical vapor deposition-grown graphene: the thinnest solid lubricant *ACS Nano* **5** 5107–14
[19] Klemenz A, Pastewka L, Balakrishna S G, Caron A, Bennewitz R and Moseler M 2014 Atomic scale mechanisms of friction reduction and wear protection by graphene *Nano Lett.* **14** 7145–52
[20] Berman D, Deshmukh S A, Sankaranarayanan S K R S, Erdemir A and Sumant A V 2014 Extraordinary macroscale wear resistance of one atom thick graphene layer *Adv. Funct. Mater.* **24** 6640–6
[21] Vasić B, Matković A, Ralević U, Belić M and Gajić R 2017 Nanoscale wear of graphene and wear protection by graphene *Carbon* **120** 137–44
[22] Filleter T, McChesney J L, Bostwick A, Rotenberg E, Emtsev K V, Seyller T, Horn K and Bennewitz R 2009 Friction and dissipation in epitaxial graphene films *Phys. Rev. Lett.* **102** 086102
[23] Amadei C A, Lai C-Y, Esplandiu M J, Alzina F, Vecitis C D, Verdaguer A and Chiesa M 2015 Elucidation of the wettability of graphene through a multi-length-scale investigation approach *RSC Adv.* **5** 39532–8
[24] Vasić B, Matković A and Gajić R 2017 Phase imaging and nanoscale energy dissipation of supported graphene using amplitude modulation atomic force microscopy *Nanotechnology* **28** 465708
[25] Molina-Mendoza A J *et al* 2017 Franckeite as a naturally occurring van der Waals heterostructure *Nat. Commun.* **8** 14409
[26] Velický M *et al* 2017 Exfoliation of natural van der Waals heterostructures to a single unit cell thickness *Nat. Commun.* **8** 14410
[27] Ray K, Yore A E, Mou T, Jha S, Smithe K K H, Wang B, Pop E and Newaz A K M 2017 Photoresponse of Natural van der Waals Heterostructures *ACS Nano* **11** 6024–30

[28] Frisenda R *et al* 2020 Symmetry breakdown in franckeite: spontaneous strain, rippling and interlayer moiré *Nano Lett.* **20** 1147–1141

[29] Alencar A B, Barboza A P M, Archanjo B S, Chacham H and Neves B R A 2015 Experimental and theoretical investigations of monolayer and few-layer talc *2D Mater* **2** 015004

[30] Barcelos I D *et al* 2018 Infrared fingerprints of natural 2D talc and plasmon? Phonon coupling in graphene? Talc heterostructures *ACS Photonics* **5** 1912–8

[31] Niu Y, Villalva J, Frisenda R, Sanchez-Santolino G, Ruiz-González L, Pérez E M, García-Hernández M, Burzurí E and Castellanos-Gomez A 2019 Mechanical and liquid phase exfoliation of cylindrite: a natural van der Waals superlattice with intrinsic magnetic interactions *2D Mater.* **6** 035023

[32] Santos J C C, Barboza A P M, Matos M J S, Barcelos I D, Fernandes T F D, Soares E A, Moreira R L and Neves B R A 2019 Exfoliation and characterization of a two-dimensional serpentine-based material *Nanotechnology* **30** 445705

[33] Leong Y W, Abu Bakar M B, Mohd Ishak Z A, Ariffin A and Pukanszky B 2004 Comparison of the mechanical properties and interfacial interactions between talc, kaolin, and calcium carbonate filled polypropylene composites *J. Appl. Polym. Sci.* **91** 3315–26

[34] Lapcik L Jr+, Jindrova P, Lapcikova B, Tamblyn R, Greenwood R and Rowson N 2008 Effect of the talc filler content on the mechanical properties of polypropylene composites *J. Appl. Polym. Sci.* **110** 2742–7

[35] Arencón D and Velasco J I 2009 Fracture toughness of polypropylene-based particulate composites *Materials* **2** 2046–94

[36] Yu F, Liu T, Zhao X, Yu X, Lu A and Wang J 2012 Effects of talc on the mechanical and thermal properties of polylactide *J. Appl. Polym. Sci.* **125** E99–109

[37] Deacon R F, Goodman J F and Bowden F P 1958 Lubrication by lamellar solids *Proc. R. Soc.* A **243** 464–82

[38] Rudenko P and Bandyopadhyay A 2013 Talc as friction reducing additive to lubricating oil *Appl. Surf. Sci.* **276** 383–9

[39] Moore D E and Lockner D A 2011 Frictional strengths of talc-serpentine and talc-quartz mixtures *J. Geophys. Res. Solid Earth* **116** B01403

[40] Hirauchi K-I, den Hartog S A M and Spiers C J 2013 Weakening of the slab-mantle wedge interface induced by metasomatic growth of talc *Geology* **41** 75–8

[41] Moore D E and Rymer M J 2007 Talc-bearing serpentinite and the creeping section of the San Andreas fault *Nature* **448** 795–7

[42] Collettini C, Niemeijer A, Viti C and Marone C 2009 Fault zone fabric and fault weakness *Nature* **462** 907–10

[43] Harvey A, Boland J B, Godwin I, Kelly A G, Szydłowska B M, Murtaza G, Thomas A, Lewis D J, O'Brien P and Coleman J N 2017 Exploring the versatility of liquid phase exfoliation: producing 2D nanosheets from talcum powder, cat litter and beach sand *2D Mater.* **4** 025054

[44] Cadore A R, Mania E, Alencar A B, Rezende N P, de Oliveira S, Watanabe K, Taniguchi T, Chacham H, Campos L C and Lacerda R G 2018 Enhancing the response of NH_3 graphene-sensors by using devices with different graphene-substrate distances *Sensors Actuators* B **266** 438–46

[45] Cappella B and Dietler G 1999 Force–distance curves by atomic force microscopy *Surf. Sci. Rep.* **34** 1–104

[46] Bennewitz R 2015 *Fundamentals of Friction and Wear on the Nanoscale* (Switzerland: Springer International Publishing) chapter Friction Force Microscopy

[47] Magonov S N, Elings V and Whangbo M-H 1997 Phase imaging and stiffness in tapping-mode atomic force microscopy *Surf. Sci.* **375** L385–91

[48] Garcia R, Gómez C J, Martinez N F, Patil S, Dietz C and Magerle R 2006 Identification of Nanoscale Dissipation Processes by Dynamic Atomic Force Microscopy *Phys. Rev. Lett.* **97** 016103

[49] Anczykowski B, Gotsmann B, Fuchs H, Cleveland J P and Elings V B 1999 How to measure energy dissipation in dynamic mode atomic force microscopy *Appl. Surf. Sci.* **140** 376–82

[50] Gorbachev R V *et al* 2011 Hunting for monolayer boron nitride: optical and Raman signatures *Small* **7** 465–8

[51] Funke S, Wurstbauer U, Miller B, Matković A, Green A, Diebold A, Röling C and Thiesen P H 2017 Spectroscopic imaging ellipsometry for automated search of flakes of mono-and n-layers of 2D-materials *Appl. Surf. Sci.* **421** 435–9

[52] Wang A, Freeman J J and Jolliff B L 2015 Understanding the Raman spectral features of phyllosilicates *J. Raman Spectrosc.* **46** 829–45

[53] Varenberg M, Etsion I and Halperin G 2003 An improved wedge calibration method for lateral force in atomic force microscopy *Rev. Sci. Instrum* **74** 3362–7

[54] Michot L J, Villieras F, Francois M, Yvon J, Le Dred R and Cases J M 1994 The structural microscopic hydrophilicity of talc *Langmuir* **10** 3765–73

[55] van Oss C J and Giese R F 1995 The hydrophilicity and hydrophobicity of clay minerals *Clays Clay Miner.* **43** 474–7

[56] Rotenberg B, Patel A J and Chandler D 2011 Molecular explanation for why talc surfaces can be both hydrophilic and hydrophobic *J. Am. Chem. Soc.* **133** 20521–7

[57] Ou X, Lin Z and Li J 2018 Surface microstructure engenders unusual hydrophobicity in phyllosilicates *Chem. Commun.* **54** 5418–21

[58] Schrader M E and Yariv S 1990 Wettability of clay minerals *J. Colloid Interface Sci.* **136** 85–94

[59] Giese R F, Costanzo P M and van Oss C J 1991 The surface free energies of talc and pyrophyllite *Phys. Chem. Miner.* **17** 611–6

[60] Thomas R R, Kaufman F B, Kirleis J T and Belsky R A 1996 Wettability of polished silicon oxide surfaces *J. Electrochem. Soc.* **143** 643

[61] Hölscher H, Ebeling D and Schwarz U D 2008 Friction at atomic-scale surface steps: experiment and theory *Phys. Rev. Lett.* **101** 246105

[62] Steiner P, Gnecco E, Krok F, Budzioch J, Walczak L, Konior J, Szymonski M and Meyer E 2011 Atomic-scale friction on stepped surfaces of ionic crystals *Phys. Rev. Lett.* **106** 186104

[63] Lee H, Lee H-B-R, Kwon S, Salmeron M and Park J Y 2015 Internal and external atomic steps in graphite exhibit dramatically different physical and chemical properties *ACS Nano* **9** 3814–9

[64] Boland M J, Nasseri M, Hunley D P, Ansary A and Strachan D R 2015 Striped nanoscale friction and edge rigidity of MoS_2 layers *RSC Adv.* **5** 92165–73

[65] Lang H, Peng Y, Zeng X, Cao X, Liu L and Zou K 2018 Effect of relative humidity on the frictional properties of graphene at atomic-scale steps *Carbon* **137** 519–26

[66] Chen Z, Khajeh A, Martini A and Kim S H 2019 Chemical and physical origins of friction on surfaces with atomic steps *Sci. Adv.* **5** eaaw0513

[67] Chen L, Chen Z, Tang X, Yan W, Zhou Z, Qian L and Kim S H 2019 Friction at single-layer graphene step edges due to chemical and topographic interactions *Carbon* **154** 67–73

[68] Vasić B, Matković A, Gajić R and Stanković I 2016 Wear properties of graphene edges probed by atomic force microscopy based lateral manipulation *Carbon* **107** 723–32
[69] Qi Y, Liu J, Zhang J, Dong Y and Li Q 2017 Wear Resistance Limited by Step Edge Failure: The Rise and Fall of Graphene as an Atomically Thin Lubricating Material *ACS Appl. Mater. Interfaces* **9** 1099–106
[70] Moore D E and Lockner D A 2004 Crystallographic controls on the frictional behavior of dry and water-saturated sheet structure minerals *J. Geophys. Res. Solid Earth* **109** B03401
[71] Escartín J, Andreani M, Hirth G and Evans B 2008 Relationships between the microstructural evolution and the rheology of talc at elevated pressures and temperatures *Earth Planet. Sci. Lett.* **268** 463–75
[72] Chen X, Elwood Madden A S and Reches Z 2017 The frictional strength of talc gouge in high-velocity shear experiments *J. Geophys. Res. Solid Earth* **122** 3661–76
[73] Smolyanitsky A, Killgore J P and Tewary V K 2012 Effect of elastic deformation on frictional properties of few-layer graphene *Phys. Rev.* B **85** 035412
[74] Sahagún E, García-Mochales P, Sacha G M and Sáenz J J 2007 Energy dissipation due to capillary interactions: hydrophobicity maps in force microscopy *Phys. Rev. Lett.* **98** 176106
[75] Tsoi S, Dev P, Friedman A L, Stine R, Robinson J T, Reinecke T and Sheehan P E 2014 van der Waals screening by single-layer graphene and molybdenum disulfide *ACS Nano* **8** 12410–7
[76] Ambrosetti A and Silvestrelli P L 2018 Hidden by graphene? Towards effective screening of interface van der Waals interactions via monolayer coating *Carbon* **139** 486–91
[77] Liu X, Zhang Z and Guo W 2018 van der waals screening by graphenelike monolayers *Phys. Rev.* B **97** 241411